



High-order OAM mode generation in a helical long-period fiber grating inscribed by an oxyhydrogen-flame

LAIPENG SHAO,¹ SHEN LIU,^{1,*}  MIN ZHOU,^{1,2} ZHENG HUANG,¹
WEIJIA BAO,¹ ZHIYONG BAI,¹  ZHAO LIU,¹ GUOXUAN ZHU,¹
ZHONGYUAN SUN,¹ JUNLAN ZHONG,¹ AND YIPING WANG¹

¹Key Laboratory of Optoelectronic Devices and Systems of Ministry of Education/Guangdong Province, College of Physics and Optoelectronic Engineering, Shenzhen University, Shenzhen 518060, China

²School of Communication and Information Engineering, Chongqing University of Posts and Telecommunications, Chongqing 400065, China

*shenliu@szu.edu.cn

Abstract: In this study, an all-fiber ± 3 -order orbital angular momentum (OAM) mode generator with $\sim 90\%$ conversion efficiency is proposed and experimentally demonstrated. By using a helical long-period fiber grating (HLPFG) inscribed by an oxyhydrogen-flame, the fundamental mode (LP_{01}) of the six-mode fiber (6MF) can be effectively converted into the OAM $_{\pm 3}$ mode without the need for polarization control. This is the first demonstration of the all-fiber ± 3 -order OAM mode generator by an oxyhydrogen-flame-induced HLPFG approach as far as we know. In addition, the broadband tunability of the ± 3 -order OAM mode generator within 1520–1630 nm is demonstrated just by changing the pitch of the helical grating. We believe that the proposed tunable ± 3 -order OAM mode generator can offer a new alternative for high-order OAM mode generation.

© 2021 Optica Publishing Group under the terms of the [Optica Open Access Publishing Agreement](#)

1. Introduction

Orbital angular momentum (OAM) beams, also known as optical vortices, are characterized by a helical phase front of $\exp(il\varphi)$, where φ and l are the azimuthal angle and the topological charge, respectively. Due to the unique helical phase structure, the OAM modes have gained substantial attention [1,2] and have been widely used in many fields, such as optical tweezing [3], optical manipulation [4], nanoscale microscopy [5], quantum optical telecommunications [6], optical fiber communication [7,8]. Up till the present moment, many efforts have been devoted to generate OAM modes, and plenty of schemes have been reported. Where the free-space OAM modes generation technique is one of the most common methods, such as phase plates [9], q-plates [10], spatial light modulators [11], silicon-integrating devices [12], *etc.* However, since the OAM mode in free space is not the fiber's eigenmodes [13], the OAM beams achieved with the above-mentioned free-space schemes in the fiber-based communication system may suffer from low mode purity. In comparison, this problem can be easily overcome by the all-fiber OAM mode generator, which possesses advantages of compact size, cost-effectiveness, high conversion efficiency, and inherent compatibility with fiber systems [14–21]. Fu *et al.* and Zhang *et al.* have successfully generated the first-order OAM modes in a HLPFG written by hydrogen-oxygen flame [18,19]. However, the potential of OAM modes to increase the capacity of fiber optical communication systems is owing to that the multiplexing multiple OAM modes can provide an additional spatial dimension to scale higher data rates. Therefore, optical devices can generate high-order OAM modes are necessary.

In recent years, a lot of schemes, e.g., cascading two long-period fiber gratings (LPGs) [17], a strong modulated LPG [15], and a HLPFG [14] have been proposed to overcome the coupling

issue between the fundamental mode and the second-azimuthal-order mode to generate the second-order OAM modes. In 2018, the fifth- and sixth-order cladding OAM modes generator based on a twisted photonic crystal fiber were demonstrated [20]. He *et al.* reported the OAM_{±3} mode generator based on an asymmetric long-period fiber grating (AS-LPFG) fabricated by multicycle scanning ablation with increased power [16]. Most recently, an approach enabling the simultaneous generation of the second- and the third-order OAM modes has been proposed and demonstrated [22]. Despite all this, developing the high-order OAM mode generator in an all-fiber system remains a pressing problem.

In this work, a high-efficiency fabrication scheme for all-fiber ±3-order OAM mode generator is proposed and experimentally demonstrated based on HLPFG written in a 6MF. The oxyhydrogen-flame setup is adopted to fabricate the HLPFG, and the fundamental mode (LP_{01}) of the 6MF can be effectively converted into the OAM_{±3} modes with ~90% conversion efficiency without the need for polarization control. To the best of our knowledge, this is the first demonstration of the all-fiber ±3-order OAM mode generator based on oxyhydrogen-flame-induce HLPFG. Besides, the broadband tunability of the ±3-order OAM mode generator within 1520-1630 nm is demonstrated just by changing the pitch of the HLPFG. The proposed method not only possesses high conversion efficiency, but also provides a new approach for exciting high-order OAM modes in HLPFGs, which may find some applications in the field of optical communications.

2. Principle and fabrication of the HLPFG

Based on the mode perturbation and mode-coupling theory, in HLPFG, the mode coupling between the fundamental mode and higher-order OAM modes needs to follow the phase matching condition of a grating and conservation of angular momentum [23]. Due to the imperfection of the fabrication, the higher-order harmonic terms of the azimuthal distribution of refractive index modulation are considered. Thus, the phase matching condition and conservation of angular momentum can be expressed as [14]:

$$n_N = n_F - m \cdot \lambda / \Lambda_0 \quad (1)$$

$$J_N = J_F + m \cdot \sigma \quad (2)$$

where n_F and n_N are the effective refractive index of LP_{01} and the high-order LP_{ij} mode, respectively. m represents the order of harmonic term, and the value of which determines the topological charge number of excited OAM mode in HLPFGs. λ is the resonant wavelength. J_F and J_N are the total angular momentum (TAM) of the two corresponding modes, respectively, which are the sums of the orbital momentum and the spin momentum of the corresponding modes, respectively. σ represents the helicity of the single HLPFG, i.e., $\sigma = 1$, and -1 represents the left- and right-hand helicity, respectively. According to Eqs. (1) and (2), the excited N th mode is then an OAM mode with a topological charge number of $m \cdot \sigma$. We can design the period Λ of the c-HLPFG to achieve mode conversion between LP_{01} and high-order LP_{ij} mode.

The optical fiber used in this work is six-mode fiber with a step-index profile, the core and cladding diameters of which are 16 and 125 μm , respectively. The supported fiber core mode profiles are obtained based on a finite-element method, as shown in Figs. 1(a₁)-(a₆). The effective indices of the modes $LP_{01} - LP_{12}$ for 6MF in terms of the different wavelengths are calculated and shown in Fig. 1(b). According to the phase matching condition of a grating and conservation of angular momentum (Eqs. (1) and (2)), the relationship between the pitches and the resonant wavelengths of the HLPFG are also calculated and shown in Fig. 1(c). The OAM-1, OAM-2, and OAM-3 modes can be obtained in the HLPFG with a certain pitch.

Figure 2 shows the fabrication experimental setup of the HLPFGs. After removing the coating, one end of the 6MF is fixed by a dual-arm fiber holder, and the other end is installed along the central axis of the rotation motor (Model QS-M42, Singapore). Simultaneously, the

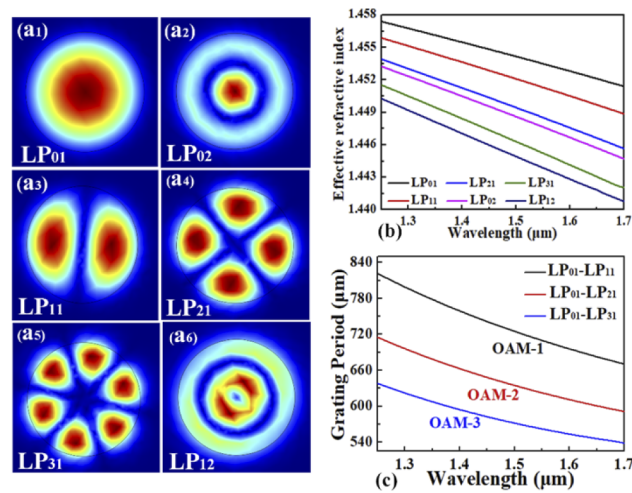


Fig. 1. (a₁)-(a₆) The 6MF supports *LP* modes: *LP*₀₁, *LP*₀₂, *LP*₁₁, *LP*₂₁, *LP*₃₁, *LP*₁₂ modes, (b) the mode dispersion curves. (c) Calculated grating pitches are required for the resonant couplings between the fundamental mode (*LP*₀₁) and high-order mode (*LP*_{*ij*}).

dual-arm fiber holder and rotation motor are fixed on two same translation stages, respectively. A hydrogen-oxygen flame is produced by a hydrogen generator (Model TH-500, China) to heat the fiber to its melting point.

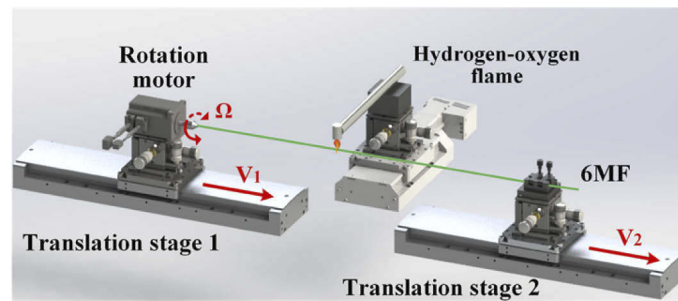


Fig. 2. Experimental setup of the fabricated HLPFGs by employing a hydrogen-oxygen flame.

A hydrogen-oxygen flame is used to heat the 6MF, and a rotation motor with a speed of Ω is employed to twist the softened fiber, that the HLPFGs can be fabricated. It should be pointed out that while writing the grating, the fiber is translated by the two translation stages with the different velocities of V_1 and V_2 ($V_2 > V_1$) simultaneously. Because of the difference between V_1 and V_2 , certain longitudinal stress will be induced and applied to the fiber, the efficiency and quality of the fabricated HLPFGs can be improved. For an HLPFG, the period Λ is jointly determined by the velocity V_2 of the translation stage 2 and the rotational speed Ω of the rotator, which can be described as

$$\Lambda = V_2 \cdot 60 / \Omega \quad (3)$$

The length of the HLPFG is

$$L = V_2 \cdot T \quad (4)$$

where T represents the heating time of the optical fiber by the hydrogen-oxygen flame. The motor's rotational direction directly determines the direction of the induced periodic helical structures in

the grating. Hence, the HLPFG can be produced by clockwise- and counterclockwise-twisted processes denoted as c-HLPFG and cc-HLPFG, respectively.

To measure the actual structure of the HLPFG achieved, we fabricate a c-HLPFG with the preparation system based on hydrogen-oxygen flame. The fabrication parameters are set as following: the rotation speed Ω is 169 rpm, and the velocities of V_1 and V_2 are 1.50 and 1.60 mm/s, respectively. The heating time is set as 60 s. Correspondingly, the period Λ and grating length L are 568.0 μm and 96 mm, respectively. A computer-controlled precision cleaving system is employed to cut the grating to the optimal length (about 27.6 mm). The transmission spectrum of the obtained grating can be measured with an optical spectrum analyzer (OSA, Model AQ6370C) and an amplified spontaneous emission (ASE) broadband light source with a wavelength ranging from 1250 to 1650 nm. The recorded transmission spectrum is shown in Fig. 3(a). A notch with a rejection depth of more than 10 dB and a 3 dB bandwidth of ~ 20.2 nm are successfully obtained at the wavelength of 1576.4 nm. The polarization-dependent loss (PDL) near the resonant wavelength of the fabricated c-HLPFG is measured (about 17.3 dB) and shown in Fig. 3(b), which may be caused by asymmetric refractive index modulation during the fabrication process.

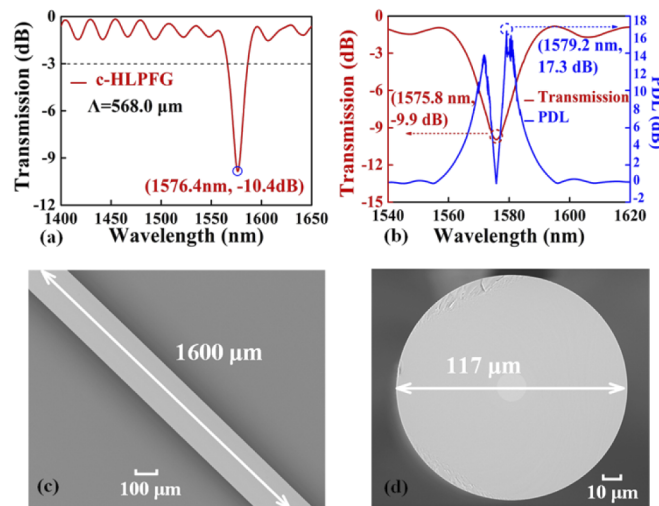


Fig. 3. (a) The transmission spectrum and (b) the PDL curve of the c-HLPFG's sample with a grating pitch of 568.0 μm . (c) The SEM along fiber axis direction and (d) SEM across-section of this sample.

Figures 3(c) and 3(d) are the scanning electron microscope (SEM) of the HLPFG along fiber axis direction and grating cross-section, respectively. It can be observed that there is no mechanical deformation on the surface of the grating, which is consistent with the result reported in Ref. [24]. This is mainly due to the large heating area and uniform heating temperature of the hydrogen-oxygen flame heating technique. The fiber diameter is decreased from 125 to 117 μm , mainly resulting from the pre-set velocity difference between the two translation stages ($V_2 - V_1 = 0.1$ mm/s).

At the same time, it is well known that topological charge transitions occur in systems with spatially perturbed refractive index distribution, where the perturbation has a helical character, as reported in Ref. [25]. The mechanism of the mode conversion to each other with different azimuthal numbers has been clarified in detail based on the theoretical model of the fiber with circular birefringence induced by torsional mechanical stress [25], which has been verified experimentally in Ref. [26]. Therefore, the HLPFG inscribed in 6MF has the potential to excite the high-order OAM mode.

3. Experimental results and discussions

In the experiment, we investigate the relationship between the period Λ of the c-HLPPFG and its resonant dip. In HLPFG based on 6MF, the LP_{01} mode can convert into any higher-order core mode by adjusting the grating parameters appropriately. According to the relationship between the pitch and the resonant wavelength of the HLPFG shown in Fig. 1(c), five c-HLPPFG samples (S_1, S_2, S_3, S_4, S_5) with the same number of grating periods (i.e., 49 grating periods) are fabricated by employing the twist rate of 166, 167, 168, 169, and 172 rpm, respectively. The obtained transmission spectra of these samples are depicted in Fig. 4(a). Each of the obtained five gratings has corresponding resonant dips (i.e., Dip 1, Dip 2, Dip 3, Dip 4, and Dip 5) with a more than -9 dB coupling strength. The resonant dips of five c-HLPPFGs with the periods of 578.3, 574.9, 571.4, 568.0, 558.1 μm are 1528.2, 1540.6, 1562.8, 1576.4, 1623.05 nm, respectively. The insertion losses are about 0.2 dB. Figure 4(b) indicates that the resonant dip of the c-HLPPFGs in the 6MF decreases vs. the period increases. According to the relationship between grating pitches required for resonant coupling of the fundamental mode (LP_{01}) and higher-order mode (LP_{ij}), the c-HLPPFGs with a desired wavelength resonant dip can be realized by changing the grating pitch of the fiber in the experiment.

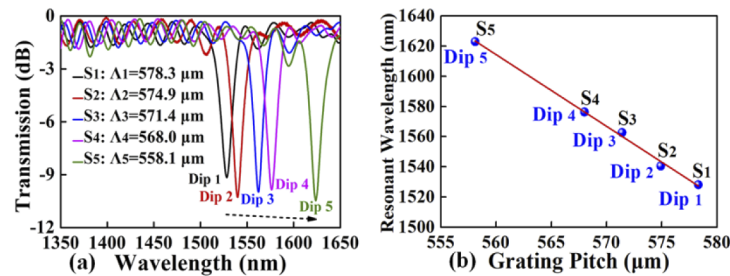


Fig. 4. (a) Transmission spectra of five c-HLPPFG samples (S_1, S_2, S_3, S_4, S_5) with different grating pitches of 578.3, 574.9, 571.4, 568.0, 558.1 μm , respectively, and (b) illustrates the measured resonant dips of the c-HLPPFGs versus grating pitch.

The c-HLPPFG (S_6) and cc-HLPPFG (S_7) with the same period of 571.4 μm and opposite directions are fabricated. The corresponding transmission spectra are shown in Fig. 5. The direction of c-HLPPFG and cc-HLPPFG does not show any remarkable influence on resonant wavelength. The difference in the coupling strength mainly results from the different lengths of the two gratings.

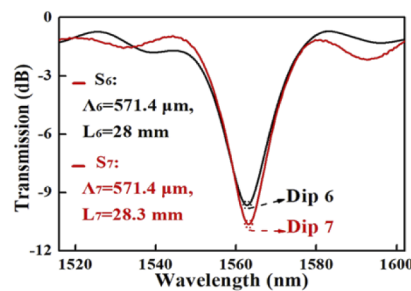


Fig. 5. Transmission spectra of the c-HLPPFG and the cc-HLPPFG sample (i.e., S_6 and S_7) with the same grating pitch of 571.4 μm .

To verify that the excited mode in the fabricated HLPFGs is $OAM_{\pm 3}$ mode. The experimental setup illustrated in Fig. 6 is employed to detect the converted modes and characterize the OAM

modes. A tunable laser (Agilent, 81940A) with a wavelength range from 1520 to 1630 nm is used as the source. The incident light from the tunable laser is split into two arms with a 3-dB coupler. One is directed into the fabricated c-HLPFG/cc-HLPFG and then collimated through the beam splitter (BS) by using an objective lens (lens1, 20x). The other is propagated into an attenuator through polarization controller (PC), and then collimated into the BS through the other lens (lens2, 20x) as a reference beam to produce the interference fringes at the imaging plane of the CCD (Electro physics Corp, Model 7290A). The PC and the attenuator are employed to adjust the visibility of the resulting interference fringes.

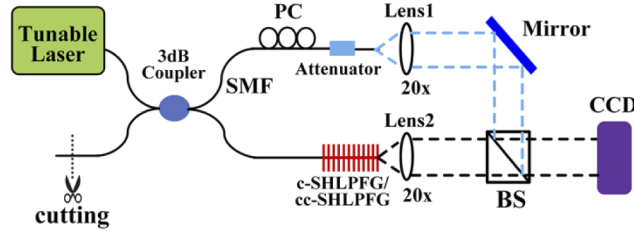


Fig. 6. Schematic diagram of the experimental setup used for detecting the converted modes and characterize the OAM modes.

When the wavelength of tunable laser is locked at the resonant dip of the c-HLPFG samples (S_1 , S_2 , S_3 , S_4 , and S_5), respectively, the experimental measurements for the mode intensity distributions and interference patterns are shown in Fig. 7. The clockwise spiral interference patterns are observed successfully at the corresponding resonant dips (1528.2, 1540.6, 1562.8, 1576.4, 1623.05 nm), respectively, which means that the c-HLPFG inscribed in 6MF can excite -3-order OAM. Consequently, the converted OAM mode could be tuned within a wide wavelength range from 1520 to 1630 nm by merely changing the grating pitch of the helical gratings.

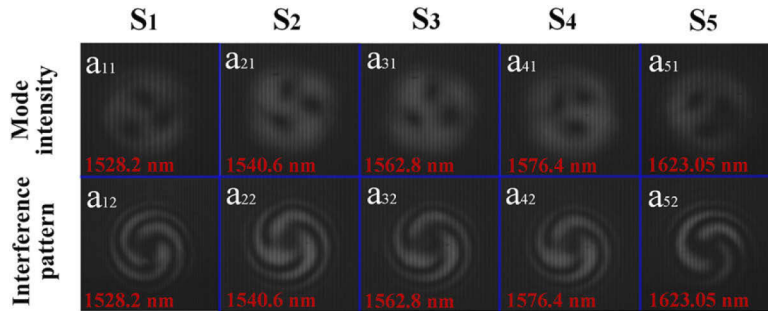


Fig. 7. (a_{11})-(a_{51}) are intensity profiles, and (a_{12})-(a_{52}) are the interference patterns for the generated OAM modes with five c-HLPFG samples at different resonant dips of 1528.2, 1540.6, 1562.8, 1576.4, 1623.05 nm, respectively.

As shown in Figs. 8(a_{62}) and 8(a_{72}), the clockwise and anticlockwise spiral interference patterns for OAM_{-3} and OAM_{+3} modes are successfully observed, which corresponding to the c-HLPFG and the cc-HLPFG samples (i.e., S_6 and S_7) at resonant dips of 1562.2 and 1563.1 nm with the same grating pitch of 571.4 μm . The above results indicate that the modes excited in HLPFG are the $OAM_{\pm 3}$ modes in our experiment. However, it can be seen from Figs. 7(a_{11})-7(a_{51}), 8(a_{61}), and 8(a_{71}) that the center of the measured mode intensity distribution of the c-HLPFG/cc-HLPFG is not a black ring, indicating that there is still Gaussian light in the center, which may be caused by the insufficient modulation of the effective refractive index. This can be improved by adjusting the preparation parameters.

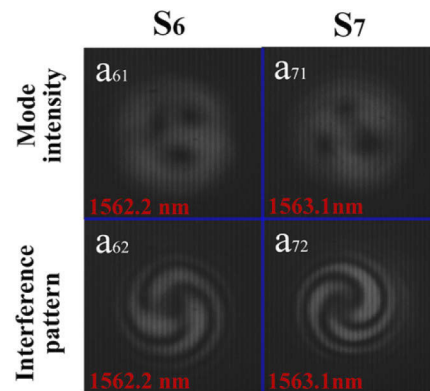


Fig. 8. (a_{61}) and (a_{71}) are the intensity profiles of the $OAM_{\pm 3}$ modes generated by c-HLPFG and cc-HLPFG samples, respectively, at a resonant dip near 1562 nm. (a_{62}) and (a_{72}) correspond to the interference patterns of c-HLPFG and cc-HLPFG, respectively.

4. Conclusions

In conclusion, we demonstrated an all-fiber high-order OAM mode generator based on a HLPFG inscribed by oxyhydrogen-flame. The ± 3 -order OAM modes are excited in the HLPFGs with a conversion efficiency of 90%, which is the first demonstration of the ± 3 -order OAM mode generator by oxyhydrogen-flame-induced HLPFG scheme as far as we know. The experimental results show that the ± 3 -order OAM modes can be obtained within the wavelength of 1520–1630 nm just by changing the pitch of the HLPFG. Therefore, the proposed tunable ± 3 -order OAM mode generator could offer a new alternative for high-order OAM mode generation.

Funding. National Natural Science Foundation of China (61905160, 61905164, 61905165, 62175165); Basic and Applied Basic Research Foundation of Guangdong Province (2018KQNCX219, 2021A1515011834); Science and Technology Planning Project of Shenzhen Municipality (RCBS20200714114922296, JCYJ20210324120403009); Postgraduate Innovation Development Fund Project of Shenzhen University (315-0000470804).

Disclosures. The authors declare no conflicts of interest.

Data availability. Data underlying the results presented in this paper are not publicly available at this time but may be obtained from the authors upon reasonable request.

References

1. A. M. Yao and M. J. Padgett, "Orbital angular momentum: origins, behaviour and applications," *Adv. Opt. Photonics*, **3**(2), 161–204 (2011).
2. C. N. Alexeyev, E. V. Barshak, B. P. Lapin, and M. A. Yavorsky, "Topological resonances, superefficient orbital-angular-momentum control, and spin-orbit-interaction enhancement in fiber-loop resonators," *Phys. Rev. A*, **101**(6), 063801 (2020).
3. M. Padgett and R. Bowman, "Tweezers with a twist," *Nat. Photonics*, **5**(6), 343–348 (2011).
4. K. Dholakia and T. Čižmár, "Shaping the future of manipulation," *Nat. Photonics*, **5**(6), 335–342 (2011).
5. S. Fürhapter, A. Jesacher, S. Bernet, and M. Ritsch-Marte, "Spiral interferometry," *Opt. Lett.*, **30**(15), 1953–1955 (2005).
6. J. Cariñe, G. Cañas, P. Skrzypczyk, I. Šupić, N. Guerrero, T. Garcia, L. Pereira, M. A. S. Prosser, G. B. Xavier, A. Delgado, S. P. Walborn, D. Cavalcanti, and G. Lima, "Multi-core fiber integrated multi-port beam splitters for quantum information processing," *Optica*, **7**(5), 542–550 (2020).
7. S. H. Li and J. Wang, "A compact trench-assisted multi-orbital-angular-momentum multi-ring fiber for ultrahigh-density space-division multiplexing (19 rings (22 modes)," *Sci. Rep.*, **4**(1), 3853 (2015).
8. N. Bozinovic, Y. Yue, Y. Ren, M. Tur, P. Kristensen, H. Huang, A. Willner, and S. Ramachandran, "Terabit-Scale Orbital Angular Momentum Mode Division Multiplexing in Fibers," *Science*, **340**(6140), 1545–1548 (2013).
9. M. W. Beijersbergen, R. P. C. Coerwinkel, M. Kristensen, and J. P. Woerdman, "Helical-wavefront laser beams produced with a spiral phaseplate," *Opt. Commun.*, **112**(5-6), 321–327 (1994).
10. L. Marrucci, C. Manzo, and D. Paparo, "Optical spin-to-orbital angular momentum conversion in Inhomogeneous Anisotropic Media," *Phys. Rev. Lett.*, **96**(16), 163905 (2006).

11. K. J. E. Curtis, B. A. Koss, and D. G. Grier, "Dynamic holographic optical tweezers," *Opt. Commun.* **207**(1-6), 169–175 (2002).
12. B. Guan, R. P. Scott, C. Qin, N. K. Fontaine, T. Su, C. Ferrari, M. Cappuzzo, F. Klemens, B. Keller, M. Earnshaw, and S. J. B. Yoo, "Free-space coherent optical communication with orbital angular, momentum multiplexing/demultiplexing using a hybrid 3D photonic integrated circuit," *Opt. Express*. **22**(1), 145–156 (2014).
13. C. W. Yeh, "Optical waveguide theory," *IEEE T Circ. Syst. Vid.* **26**(12), 1011–1019 (1979).
14. H. Zhao, P. Wang, T. Yamakawa, and H. P. Li, "All-fiber second-order orbital angular momentum generator based on a single-helix fiber grating," *Opt. Lett.* **44**(21), 5370–5373 (2019).
15. H. Wu, S. C. Gao, B. S. Huang, Y. H. Feng, X. C. Huang, W. P. Liu, and Z. H. Li, "All-fiber second-order optical vortex generation based on strong modulated long-period grating in a four-mode fiber," *Opt. Lett.* **42**(24), 5210–5213 (2017).
16. X. D. He, J. J. Tu, X. W. Wu, S. C. Gao, L. Shen, C. L. Hao, Y. H. Feng, W. P. Liu, and Z. H. Li, "All-fiber third-order orbital angular momentum mode generation employing an asymmetric long-period fiber grating," *Opt. Lett.* **45**(13), 3621–3624 (2020).
17. Y. H. Zhao, Y. Q. Liu, C. Y. Zhang, L. Zhang, G. J. Zheng, C. B. Mou, J. X. Wen, and T. Y. Wang, "All-fiber mode converter based on long-period fiber gratings written in few-mode fiber," *Opt. Lett.* **42**(22), 4708–4711 (2017).
18. Y. Zhang, Z. Y. Bai, C. L. Fu, S. Liu, J. Tang, C. R. Liao, Y. Wang, J. He, and Y. P. Wang, "Polarization-independent orbital angular momentum generator based on a chiral grating," *Opt. Lett.* **44**(1), 61–64 (2019).
19. C. L. Fu, S. Liu, Z. Y. Bai, J. He, C. R. Liao, Y. Wang, Z. L. Li, Y. Zhang, K. M. Yang, B. Yu, and Y. P. Wang, "Orbital angular moment mode converter based on helical Long Period Fiber Grating inscribed by Hydrogen-Oxygen Flame," *J. Lightwave Technol.* **36**(9), 1683–1688 (2018).
20. C. L. Fu, S. Liu, Y. Wang, Z. Y. Bai, J. He, C. R. Liao, Y. Zhang, F. Zhang, B. Yu, S. C. Gao, Z. H. Liu, and Y. P. Wang, "High-orbital angular momentum mode generator based on twisted photonic crystal fiber," *Opt. Lett.* **43**(8), 1786–1789 (2018).
21. M. Zhou, Z. zhang, L. P. Shao, S. Liu, Y. Liu, Y. Pang, Z. Y. Bai, C. L. Fu, W. Cui, L. Qi, and Y. P. Wang, "Broadband tunable orbital angular momentum mode converter based on a conventional single-mode all-fiber configuration," *Opt. Express* **29**(10), 15595–15603 (2021).
22. T. Detani, H. Zhao, P. Wang, T. Suzuki, and H. Li, "Simultaneous generation of the second- and third-order OAM modes by using a high-order helical long-period fiber grating," *Opt. Lett.* **46**(5), 949–952 (2021).
23. M. Napiorkowski and W. Urbanczyk, "Role of symmetry in mode coupling in twisted microstructured optical fibers," *Opt. Lett.* **43**(3), 395–398 (2018).
24. Z. L. Li, S. Liu, Z. Y. Bai, C. L. Fu, Y. Zhang, Z. Y. Sun, X. Y. Liu, and Y. P. Wang, "Residual-stress-induced helical long period fiber gratings for sensing applications," *Opt. Express* **26**(18), 24114–24123 (2018).
25. E. Barshak, C. Alexeyev, B. Laipin, and M. Yavorsky, "Twisted anisotropic fibers for robust orbital-angular-momentum-based information transmission," *Phys. Rev. A.* **91**(3), 033833 (2015).
26. M. Bernas, K. Zolnacz, M. Napiorkowski, G. Statkiewicz, and W. Urbanczyk, "Conversion of LP11 modes to vortex modes in a gradually twisted highly birefringent optical fiber," *Opt. Lett.* **46**(18), 4446–4449 (2021).